Application of sinusoidal field pole in a permanent magnet synchronous machine to improve the acoustic behavior considering the MTPA and MTPV operation area

Aryanti Kusuma Putri, Sebastian Rick, David Franck and Kay Hameyer
Institute of Electrical Machines
RWTH Aachen University
Email: aryanti.putri@iem.rwth-aachen.de

***Abstract*—In this paper, various approaches to improve the acoustic behavior of a single layer interior permanent magnet synchronous machine (IPMSM) are evaluated. The studied machine is designed for the application in electric vehicles and has a maximum output power of 53.6 kW. The acoustic noise of the electrical machine is mainly generated due to vibration of the stator yoke, which is caused by the radial forces acting on the stator's teeth. The radial force is directly correlated with the flux density in the air gap. Through modification of the outer frame of the rotor, the composition of the air gap field, which consists of the fundamental wave and its harmonics, can be modified. The distribution of the radial force density on the surface of the stator teeth will be affected and the dominant order of the radial force can be reduced selectively, which will improve its acoustic behavior.**

***Index Terms*—PMSM, acoustic and noise of electrical machines, air gap flux, sinusoidal field pole, rotor pole shaping, torque harmonics, force densities, electric vehicles**

I. Introduction

The role of electric vehicles in individual transportation has become significant in the recent years. Although electrical drives are known for the low noise emission when compared to combustion engine, significant acoustic problems originated from single tones attract particular attention. Combustion engines, in contrast to the electric motor, generate broadband noise. Noise from electric motor has a single tone characteristic and lies within the sensitive hearing range of humans, which is generally between 2-5 kHz [1]. The sound radiation is strongly dependent on the housing and the installation of the machine. For a feasible acoustic evaluation, these aspects have to be considered. Therefore, structural dynamic and acoustic simulations have to be performed [2]. However, in the case that the dominant frequencies of the acoustic radiation are known, it is sufficient to analyze the exciting forces for the improvement of the electrical drive.

The major sources of noise in electrical machines are the periodic radial and tangential forces waves acting on stator and rotor respectively. The radial forces acting on the stator lead to the deformation of the housing. The tangential forces acting on the rotor leads to torque and torque pulsation. Both result in unwanted vibration of the machine parts, e.g. shaft, gearing, and differential, which is followed by acoustic radiation. Since the sum of the torque depends on the integration of tangential forces and the axial length, the pulsation can be reduced by skewing the stator or rotor. The sum of the radial forces on the stator circumference in a time step is null. In this case, the local force densities distribution have to be analyzed. The local force densities are related to the flux density waves on the air gap. As example in an induction machine with a squirrel cage rotor, these harmonics can be reduced by choosing specific numbers of stator and rotor slots [3]. In a salient pole synchronous machine, the flux density harmonics can be reduced by altering the pole shoe shape of the rotor [4].

In this paper, a systematic approach to minimize the flux density harmonics of the air gap to reduce the acoustic radiation of an interior permanent magnet synchronous machine (IPMSM) is presented. The focus of this work lies on the improvement of the electromagnetic circuit through forming the rotor's surface and thus the shape of the airgap. The stator, housing and other machine components are not altered, so the time consuming structural dynamic and acoustic simulations can be avoided. The resulting torque harmonics (temporal), which represent the sum of tangential force waves (spatial), and radial force density waves (temporal and spatial) are analyzed. The velocity on the stator surface caused by the radial force density waves acting on the stator teeth is evaluated. The proposed method is applied in a nonskewed single layer interior permanent magnet synchronous machine (IPMSM). The simulation and machine parameters are listed in Table I. The results are analyzed for the entire operating area, which is defined through maximal torque per ampere (MTPA) in base speed and maximal through per voltage (MTPV) in field weakening operating points [5].

TABLE I: Simulation and Machine Parameters of the IPMSM

Stator outer radius $r_{stator,o}$	90 mm
Stator inner radius $r_{stator,i}$	61 mm
Air gap length δ	0.7 mm
Axial length l_{Fe}	120 mm
Number of Poles / Slots $2p/N$	12 / 36
Battery voltage U_{dc}	300 V
Maximum current (peak value) I_{max}	300 A
Rated torque M_N	155 Nm
Rated speed n_N	3300 min^{-1}
Rated power P_N	53.6 kW

978-1-4799-7941-7/15/$31.00 ©2015 IEEE

II. METHODOLOGY

A. Analysis of the Radial Force Density Waves

The radial force density waves acting on the stator teeth are the major reason of the vibration of the stator's teeth, which leads to the deformation of the stator yoke. These force density waves can be traced back to the harmonics of flux densities, which originate from the rotor or stator. Generally, the flux density harmonics are caused by permanent magnets, stator slots and winding, and other effects such as saturation and eccentricity. The radial force density waves $\sigma_{rad}(\alpha, t)$ can be calculated with the simplified equation [6]:

$$\begin{aligned}\sigma_{rad}(\alpha,t) &= \frac{B_{rad}(\alpha,t)^2}{2\,\mu_0} \\ &= \frac{B_1(\alpha,t)^2 + 2\,B_1(\alpha,t)\,B_2(\alpha,t) + B_2(\alpha,t)^2}{2\,\mu_0},\end{aligned} \tag{1}$$

whereas α and t describe the position in the airgap and point in time. μ_0, B_{rad}, B_1 and B_2 are magnetic constant, sum of radial flux density in the airgap, radial flux density from stator and rotor respectively. After [7], the force density waves described in (1) can be decomposed according to its source of flux density waves. The force densities with r-th spatial order $\sigma_{rad,r}$, which occur due to the flux density harmonics of stator or rotor in combination with itselves, are described with the equation:

$$\sigma_{rad,r}(\alpha,t) = \frac{B_{rad,\nu/\mu}(\alpha,t)^2}{2\,\mu_0} \tag{2}$$

The force densities with r-th spatial order $\sigma_{rad,r}$, which occur due the combination of the flux density harmonics of stator and rotor, are described with the equation:

$$\sigma_{rad,r}(\alpha,t) = \frac{2\,B_{rad,\nu}(\alpha,t)\,B_{rad,\mu}(\alpha,t)}{2\,\mu_0}. \tag{3}$$

$B_{rad,\nu}$ and $B_{rad,\mu}$ are radial flux density ν-th order from stator and μ-th order from rotor (spatial) respectively. The deformation's amplitude r-th spatial order Y_r of the stator yoke, which is caused by these force densities, can be estimated with the equations [3]:

$$\begin{aligned}Y_0 &= -\frac{r_{stator,i}\,N_{yoke}}{E_{Fe}\,h_{yoke}}\sigma_{rad,0} \\ Y_1 &= \frac{4}{3}\frac{r_{stator,i}\,l_{Fe}}{E_{Fe}\,(\frac{d_{shaft}}{L_{shaft}})^4\,L_{shaft}}\sigma_{rad,1} \\ Y_{r>=2} &= Y_0\,(\frac{2\sqrt{3}\,N_{yoke}}{h_{yoke}}\frac{1}{r^2-1})^2\,\sigma_{rad,r}.\end{aligned} \tag{4}$$

d_{shaft} and L_{shaft} are the diameter of the shaft and the distance of the bearings respectively. Assuming that the deformation of the stator is an oscillation in stationary state, the surface velocities $\dot{Y}$ can be calculated with:

$$\dot{Y}_r = 2\,\pi\,f_{mech}\,s\,Y_r, \tag{5}$$

whereas f_{mech} and s are the mechanical rotation frequency and temporal order respectively. The deformation of the stator yoke depending on spatial order r is illustrated in Fig. 1. A deformation with spatial order r rotates with the frequency $f_{mech} * s$ and produces a tone with the same frequency. It is shown in (4), that the amplitude of the stator deformation Y_r decreases with $1/r^4$. Therefore, the relevant radial force densities, i.e. force density waves with low spatial order, correspond to the dominant amplitude of the stator deformation and thus its surface velocity. Hence, it is sufficient to analyze the amplitude of stator deformation or the surface velocity to determine the force densities, which are prominent to the acoustic radiation.

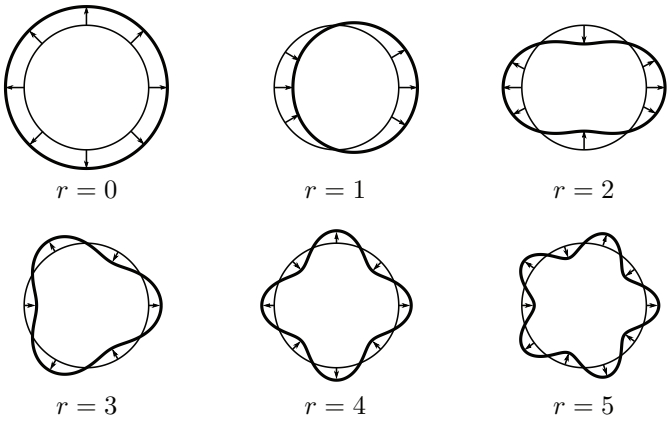

Fig. 1: The deformation of the stator yoke depending on spatial order r.

Through convolution of a radial force density wave, the time and spatial orders of the flux densities, which have major contribution to the radial force density, can be determined [8]. The terms in (1) can be two-dimensional (2D) Fourier transformed and the equation can be rewritten in:

$$\sigma_{DFT2}(s,r) = \frac{B_{DFT2}(\nu/\mu,s) * B_{DFT2}(\nu/\mu,s)}{2\,\mu_0}. \tag{6}$$

The Fourier transformed force and flux densities (σ_{DFT2} and B_{DFT2} respectively) are dependent on temporal order s and spatial orders:

- of the force density waves r,
- of the flux density waves originated from stator ν,
- of the flux density waves originated from rotor μ.

To determine the origin of the flux density waves, finite element simulations (FE-simulations) of rotor with magnetic ideal slotless stator or stator with magnetic ideal rotor ($\mu_r \to \infty$ or Neumann boundary condition) need to be performed. As a result, the source of flux density harmonics in the air gap can be separated.

B. Analysis of the Tangential Force Density Waves

According to [9], the sum of the forces F_k on every node k (nodal force) multiplied by its distance to the origin of the rotor r_k represent the torque T in one point in time. It is described with the equation:

$$T = \Sigma\,r_k \times F_k. \tag{7}$$

Due to the cross product, only the tangential nodal forces have influence on the torque. Through implementation of (7) for multiple time steps up to one rotation of the rotor, the mean torque and torque harmonics can be calculated. Through analyzing the time-dependent torque, the effect of the tangential force densities wave can be studied.

C. Implementation

The first step of the approach is to perform FE-simulations to determine the nodal forces on the air gap side of the stator's surface. The force density waves acting on the stator are calculated through averaging two neighboring nodal forces (Fig. 2) and dividing its value by the distance between the two nodes and the axial length of the machine. The force densities should be decomposed in radial and tangential components. Through 2D Fourier transformation, the force densities can be decomposed in temporal and spatial order. As shown in Fig. 2, the average of nodal forces and thus the force density waves point mainly in radial direction. The value of the force densities in radial direction is greater than its value in the tangential direction. For this reason, it is sufficient to analyze only the radial force density waves to prognose the acoustic behavior of the machine. In case the acoustic radiation is excited by the torque harmonics, the correlated radial force density waves (temporal order) should be analyzed.

The next step is to determine the radial force density waves, which have major contribution to the acoustic radiation. It can be determined through measurement of sound pressure level (SPL) or estimated through simulation. By measuring the SPL, the dominant temporal orders of the acoustic radiation can be determined. The lowest spatial order of these temporal orders should be chosen for further study. Without measurement results, the dominant excitation of the acoustic radiation can only be estimated. Generally, the pair of dominant torque harmonics (temporal order) with the lowest spatial order should be chosen. Furthermore, the dominant force density waves with low temporal and spatial order should be analyzed.

The chosen force density waves are convoluted to identify the flux density waves, which have major contribution to these force densities. Depending on the result, the rotor and stator geometry or its winding can be altered to minimize the flux density harmonics in the air gap. This paper focuses on the flux density originated from the rotor and the alteration is performed on the outer surface of the rotor.

III. Alteration of Rotor's Surface

In this section two approaches to reduce flux density harmonics by alternating the outer surface of the rotor will be introduced. The first approach is using the sinusoidal rotor field poles calculated with inverse cosine formula. The second approach is the notching of rotor's surface in d- or q-axis. The method to evaluate the influence of rotor's alteration on the air gap flux density is described at the end of the section.

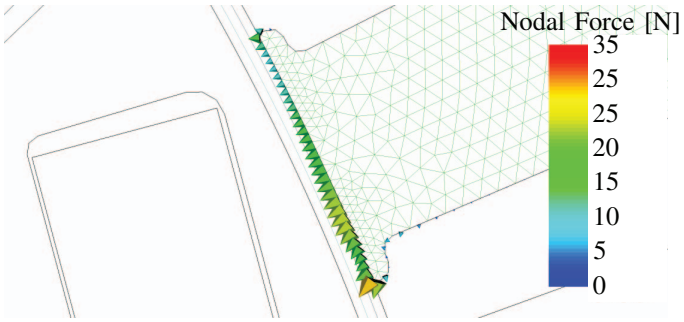

Fig. 2: The average of nodal forces between two neighboring nodes.

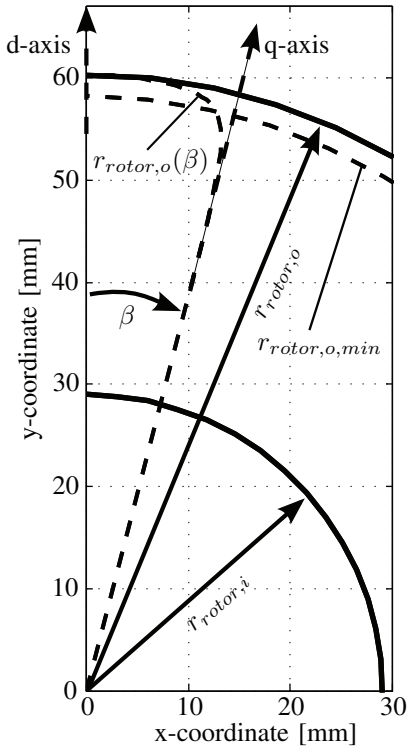

Fig. 3: Illustration of sinusoidal field pole and its parameters.

A. Sinusoidal Rotor Field Poles

Through methods introduced in [4] the harmonics of air gap flux densities can be reduced and sinusoidal rotor field can be reached. The alteration of the rotor's surface is defined with the equations:

$$\delta(\beta) = \frac{\delta_d}{cos(\frac{\pi}{\tau_p}\beta)} \tag{8}$$

$$r_{rotor,o}(\beta) = r_{rotor,o} + \delta_d - \delta(\beta), \tag{9}$$

whereas δ_d is air gap length in the d-axis, τ_p is the pole pitch, β is the angle relative to d-axis of the rotor, $\delta(\beta)$ and $r_{rotor,o}(\beta)$ are the air gap length and rotor outer radius dependent on β respectively. In Fig. 3 a half of a rotor pole is shown and the parameters in (8) and (9) are illustrated. According to the previous equations, the rotor outside radius should follow the dashed contour pointed by $r_{rotor,o}(\beta)$. This parameter is limited with the rotor minimal outside radius $r_{rotor,o,min}$ and hence the air gap length in the q-axis δ_q. The ratio of the air gap length in q- and d-axis δ_q/δ_d is varied and its influence on the flux density composition is evaluated.

B. Notching of Rotor's Surface

As an alternative to the previous section, the modifications of rotor surface on the d- and q-axis are considered. The cogging torque of an IPMSM can be reduced by notching the rotor surface in the d-axis [10] or q-axis [11]. The notch parameters are shown in Fig. 4, which are notch angle to d- or q-axis α_{notch} and notch depth d_{notch}. The influence of both parameters on the flux density harmonics is evaluated separately.

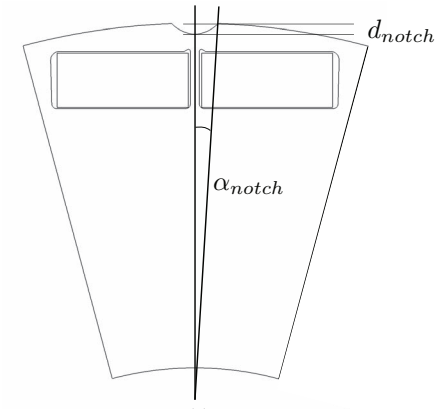

(a)

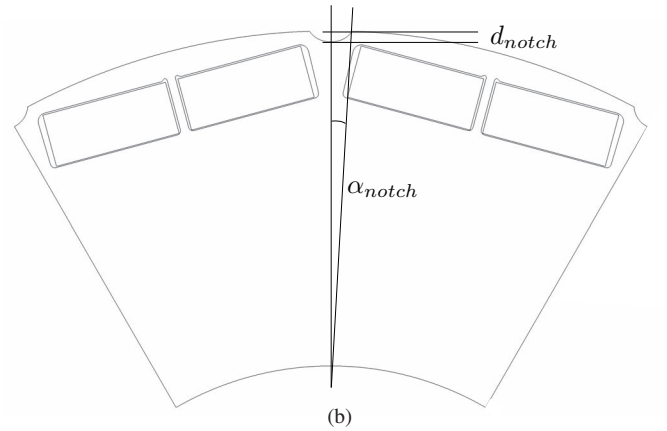

(b)

Fig. 4: Notch on d-axis (a) or q-axis (b).

C. Evaluation of Flux Density Waves

The flux density harmonics originated from rotor are evaluated. The stator is treated as an ideal slotless stator, which is implemented in the FE-simulation by applying neumann boundary condition on the stator inner radius. With this method, there is only one time step required for the analysis of the flux density, since in this case the flux density is not time-dependent. The flux density in the middle of the airgap $r_{\delta,mid} = 60,65\,\mathrm{mm}$ is sampled and Fourier transformed (spatial). The total harmonic distortion (THD) is evaluated with the equation:

$$THD = \sqrt{\frac{\sum\limits_{\mu>1} B_{rad,\mu}^2}{\sum\limits_{\mu} B_{rad,\mu}^2}}. \tag{10}$$

The objective of the rotor's surface alteration is to reduce the spatial flux density harmonics without reducing the fundamental wave significantly. In addition, the lower harmonics of the flux density have a major effect on the parasitic effects. Thus, the reduction of lower harmonics has a higher priority than recution of the higher harmonics. Therefore, the evaluation criteria of the flux density harmonics are:

- the total harmonic distortion,
- the value of the flux density's fundamental wave,
- the value of the flux density's harmonics $\mu = 3, 5, 7$.

IV. Application on the IPMSM

The methods, which are explained in the previous sections, are applied to the examined IPMSM. First of all, the relevant operating points for the analysis have to be chosen. To examine the forces acting on the rotor, the torque harmonics have to be analyzed. The first dominant torque harmonic of the examined IPMSM is the 36^{th} harmonic, which is the first slot harmonics. In Fig. 5 the characteristic torque-speed-diagram of this harmonic is shown. From the diagram could be concluded, that the maximum of this harmonic is located at the maximum torque in the base speed area. The amplitude is 30 Nm, which represents 20 % of the average torque. The operating point between base speed and field weakening area ($n = 3300\,\mathrm{min}^{-1}$ and $M = 155\,\mathrm{Nm}$) at rated operating point is chosen for further examination.

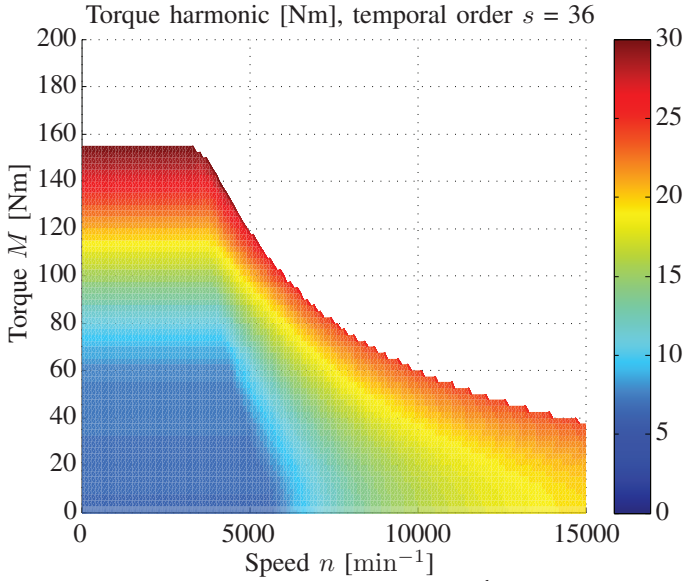

Fig. 5: Characteristic torque-speed-diagram of the 36^{th} harmonic of torque.

To examine the radial forces, which cause the deformation of the housing, the radial force density waves have to be analyzed. The low spatial orders r with highest value of the force densities have to be chosen. According to [7], the dominant force density orders of the examined machine are (temporal s, spatial r): (12, 12), (24, -12) and (36, 0). In Fig. 6 the characteristic torque-speed-diagramm for the radial force density order (36, 0) is shown. The operating points with the highest force density value are chosen for further examination. The chosen operating points for the three aforementioned force density orders are listed in Table II. Calculation of surface velocities will be performed on these operating points.

In Fig. 7 the calculated surface velocities on the stator surface are shown. In all studied operationg points, the surface velocity reaches its maximum at temporal order $s = 36$ and

TABLE II: Operating Points for Calculation of Surface Velocities

Force density orders (s, r) [kN/m^2]	Speed n [min^{-1}]	Torque M [Nm]	Current I_{eff} [A]	Control angle ψ [°]
$\sigma_{DFT2}(12, 12) = 200$	3300	155	210	-30
$\sigma_{DFT2}(24, -12) = 22.2$	8000	30	95	-70
$\sigma_{DFT2}(36, 0) = 36$	7400	82.5	200	-70

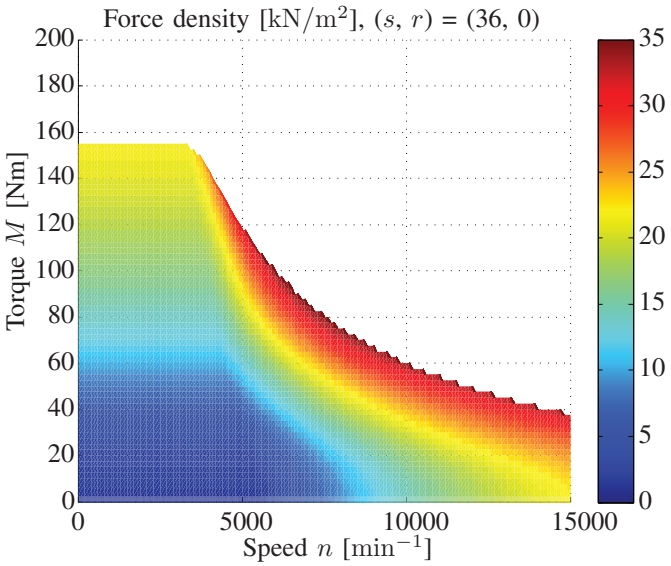

Fig. 6: Characteristic torque-speed-diagram of the force density wave order (temporal s, spatial r) = (36, 0).

spatial order $r = 0$. The next dominant orders are (s, r) = (72, 0) and (s, r) = (12, 12). It is shown, that the values of the force densities are not directly correlated with the surface velocities, and therefore the acoustic radiation. The acoustic radiation is strongly dependent on the temporal and spatial order of the force excitations. The frequencies of the noise excited from the force density order $(s, r) = (36, 0)$ between the speed $n = 3300 - 8000\,\mathrm{min}^{-1}$ lie between $f = 1980 - 4800\,\mathrm{Hz}$. These frequencies are located in the area of the human sensitive hearing range. To improve the acoustic behavior of the IPMSM this force density order have to be reduced. The operating point $n = 7400\,\mathrm{min}^{-1}$ and $M = 82.5\,\mathrm{Nm}$ shows the highest surface velocity order (36, 0), when compared to the other operating points. This radial force density order in the correspondent operating point will be convoluted to determine the contributing flux densities.

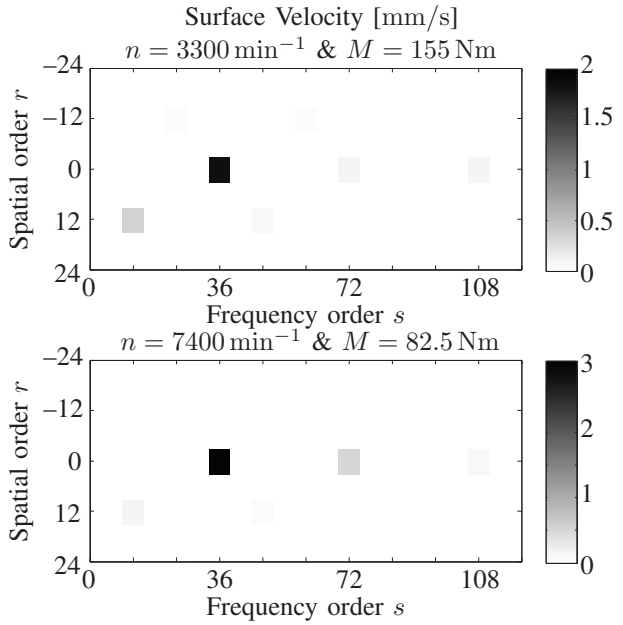

Fig. 7: The excited surface velocities at two operating points.

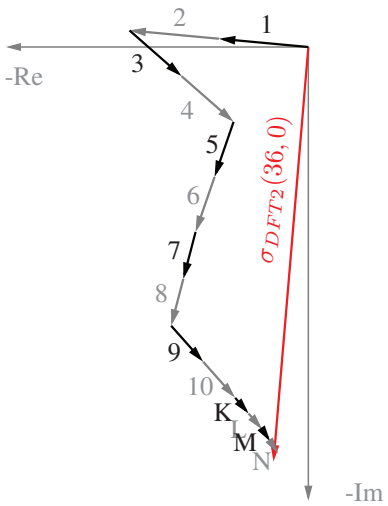

Fig. 8: Space vector convolution of the force density order (36,0) at operating point $n = 7400\,\mathrm{min}^{-1}$ and $M = 82.5\,\mathrm{Nm}$.

TABLE III: Contributing Flux Density Orders

Vector number	Flux Density Pair $B_{rad}(s,r)$	Flux Density Pair $B_{rad}(s,r)$
1 & 2	6, 6	30, -6
3 & 4	42, 42	6, -42
5 & 6	6, -6	42, 6
7 & 8	30, 30	6, -30
9 & 10	18, 18	18, -18
K & L	18, -18	54, 18
M & N	54, 54	18, -54

In Fig. 8 the decomposition of the radial force density order (36, 0) ($\sigma_{DFT2}(36, 0)$) into its constructing force densities (numbered arrows) is shown. The vectors are sorted in descending order after their absolute value. The pairs of the flux density orders, which build each force density vectors, are listed in Table III. The flux densities order (6, 6), (18, 18), (30, 30), (42, 42) and (54, 54) are originated from rotor. The normed orders (after polepair p and simulation of a time step) are 1^{st}, 3^{rd}, 5^{th}, 7^{th} and 9^{th} respectively. The fundamental wave is the order (6, 6) or the 1^{st} order. The value of the higher harmonics have to be reduced, to improve the acoustic behavior. The objective is to alter the rotor flux density of the IPMSM into a sinusoidal form, as shown in Fig. 9. In the next subsections, the rotor alteration will be performed and its effect on the flux density will be examined.

A. *Sinusoidal Rotor Field Poles*

Simulations of rotors with varied air gap ratio $\delta_q/\delta_d = 1-3$ with an increment of 0.25 are performed. The minimum width of the bridge between the magnet and rotor outside contour is set to 0.3 mm. To meet this condition, the position of the magnets relative to rotor outside contour will be changed and their geometry are kept constant. The results are shown in Table IV. It is shown, that the THD of the air gap flux density decreases significantly until the air gap ratio $\delta_q/\delta_d = 2$ is reached. The harmonics sink remarkably until the air gap ratio $\delta_q/\delta_d = 1.75$. The fundamental wave of the flux density increases and reaches its maximum between $\delta_q/\delta_d = 2-2.75$. In Fig. 9 the spatial distribution of the flux densities for $\delta_q/\delta_d = 2\,\&\,2.25$ are shown. They are compared to the flux

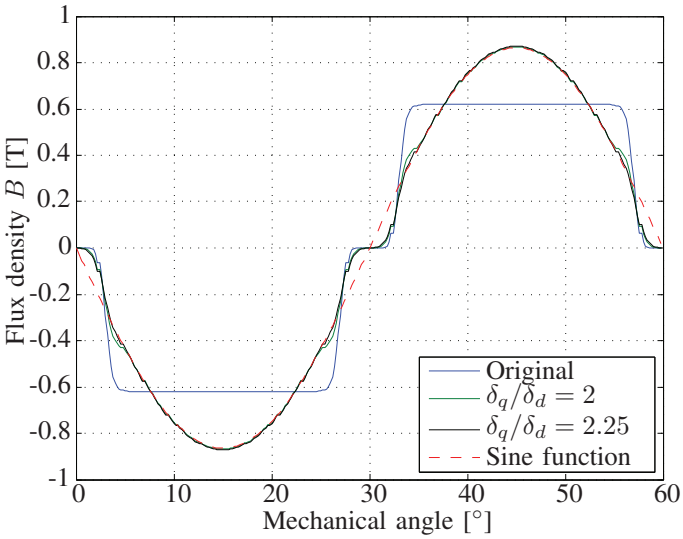

Fig. 9: The air gap flux density of IPMSM rotor with and without sinusoidal field poles.

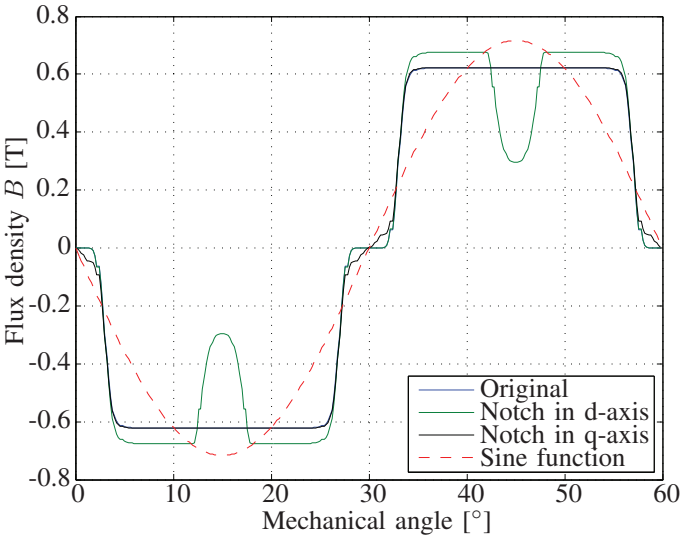

Fig. 10: The air gap flux density of IPMSM rotor with and without notch in d- or q-axis.

TABLE IV: Variation of air gap ratio δ_q/δ_d

Air gap ratio	THD	Flux density order [T]				
δ_q/δ_d	[%]	1	3	5	7	9
1 (Original)	24.38	0.75	0.15	0.01	0.06	0.07
1.25	17.73	0.77	0.09	0.02	0.05	0.07
1.5	11.81	0.80	0.04	0.01	0.03	0.06
1.75	8.54	0.84	0.01	0	0.03	0.04
2	6.91	0.86	0.01	0.02	0.03	0.03
2.25	6.42	0.86	0.02	0.02	0.03	0.03
2.5	6.23	0.86	0.02	0.03	0.03	0.02
2.75	5.98	0.86	0.02	0.03	0.03	0.02
3	5.53	0.85	0.02	0.02	0.02	0.02

density of the original IPMSM and a sine function. It is shown in the distribution, that the flux densities sampled at $\pm 10°$ from d-axis follow the sine function thoroughly. The difference between the two sinusoidal poles are insignificant. Due to the wider range of the similarity to the sine function, the rotor with air gap ratio $\delta_q/\delta_d = 2.25$ is chosen for further examination.

B. Notching of Rotor's Surface

The variation of the notch parameters (angle α_{notch} and depth d_{notch}) in d- and q-axis are performed. The minimum width of the bridges is kept at 0.3 mm and the magnets' position isn't changed. In Fig. 10 the spatial distribution of the flux densities with notch in d- or q-axis are shown. The notch in d-axis causes a drop of the flux density in the position of the notch. The notch in q-axis induces a smoother transition of the flux density between the poles. The simulation results are listed in Table V and Table VI. It is shown, that the notch in the d-axis induces a lower fundamental wave of flux densities when compared to a rotor with a notch in q-axis. In both cases, the THD of the flux densities are higher than the original model. The value of the 7^{th} harmonic order can be lowered with both notch's position. The 9^{th} harmonic order is additionally lowered in case of a notch in q-axis. The gray rows mark the geometry with highest reduction the 7^{th} harmonic order, which has vast contribution to the flux density order (36, 0) at $n = 7400\,\text{min}^{-1}$ and $M = 82.5\,\text{Nm}$ (Table III). These geometries are chosen for further examination.

TABLE V: Variation of Notch Parameters α_{notch} & d_{notch} in d-Axis

Angle	Depth	THD	Flux density order [T]				
α_{notch} [°]	d_{notch} [mm]	[%]	1	3	5	7	9
0.9	0.25	26.63	0.74	0.16	0.02	0.05	0.09
0.9	2	29.47	0.74	0.18	0.04	0.04	0.10
0.5	0.5	25.73	0.75	0.15	0.01	0.06	0.07
2	0.5	32.48	0.73	0.2	0.06	0.02	0.1
1.5	0.5	30.11	0.74	0.19	0.04	0.03	0.01
2.5	1	38.22	0.72	0.25	0.09	0.01	0.12
4	1.5	49.44	0.68	0.34	0.13	0.03	0.08
5	1.75	55.64	0.66	0.39	0.13	0.08	0.04

TABLE VI: Variation of Notch Parameters α_{notch} & d_{notch} in q-Axis

Angle	Depth	THD	Flux density order [T]				
α_{notch} [°]	d_{notch} [mm]	[%]	1	3	5	7	9
0.9	0.5	23.38	0.75	0.15	0.01	0.06	0.07
0.9	4	23.73	0.76	0.17	0.02	0.03	0.04
0.5	2.5	24.25	0.75	0.15	0	0.06	0.07
1	2.5	28.84	0.81	0.2	0.08	0.01	0.02
0.5	1.5	24.37	0.75	0.15	0.01	0.06	0.07
1	2.5	23.90	0.75	0.15	0	0.05	0.06
1.5	4	26.67	0.79	0.20	0.07	0.01	0.01
2	3.5	29.78	0.81	0.23	0.09	0.03	0

C. Combination of Presented Approaches

As shown in Fig. 9 and Fig. 10, the combination of sinusoidal field poles and notches in q-axis show the most promising results. Through the sinusoidal field pole, the flux density near d-axis follow the shape of a sine function. The notch in q-axis leads to a smoother transition between the poles. The chosen air gap ratio $\delta_q/\delta_d = 2.25$ and notch angle $\alpha_{notch} = 2°$ are implemented on the rotor. The chosen angle corresponds to the half of the pole transition angle in the flux density distribution. The depth of the notch d_{notch} is 3,5 mm, which is the maximum depth subjected to the condition of minimum width of the bridges. In this case, the value of the fundamental wave is 0.89 T, the THD is 1.69 %, and the value of the rest of the harmonics are under 0.005 T.

V. Results

A. Analysis of an Operating Point

Simulations for the operating point with siginificant surface velocities ($I_{eff} = 200\,\mathrm{A}$ & $\psi = -70°$) for the chosen geometries are performed. The results are listed in Table VII. It is shown, that sinusoidal field pole and notch in q-axis are effective to reduce the surface velocity, and thus the acoustic emission. Due to change of the reluctance, the effective torque of these variants is reduced, particularly of the rotor with notch in q-axis. However, the torque harmonics are also decreased. The notch in d-axis doesn't have considerable advantage to torque and noise production. The combination of sinusoidal field pole and notch in q-axis shows the best noise emission and proportion of mean torque and its harmonics. This geometry will be examined for the entire operating area.

TABLE VII: Simulation results $I_{eff} = 200\,\mathrm{A}$ & $\psi = -70°$

Rotor alteration	$\sigma_{DFT2}(36,0)$ [kN/m^2]	$\dot{Y}(36,0)$ [mm/s]	M_{mean} [Nm]	$\frac{M_{harm}}{M_{mean}}$ [%] 36	72
Original	36	3.1	83.4	30.0	4.9
Sinusoidal Field Pole (SFP)	20	1.7	76.3	25.2	1.3
Notch in d-axis	34	2.9	78.2	39.1	5.8
Notch in q-axis	17	1.5	66.0	11.0	4.0
Combination SFP & q-notch	14	1.2	70.4	13.3	1.3

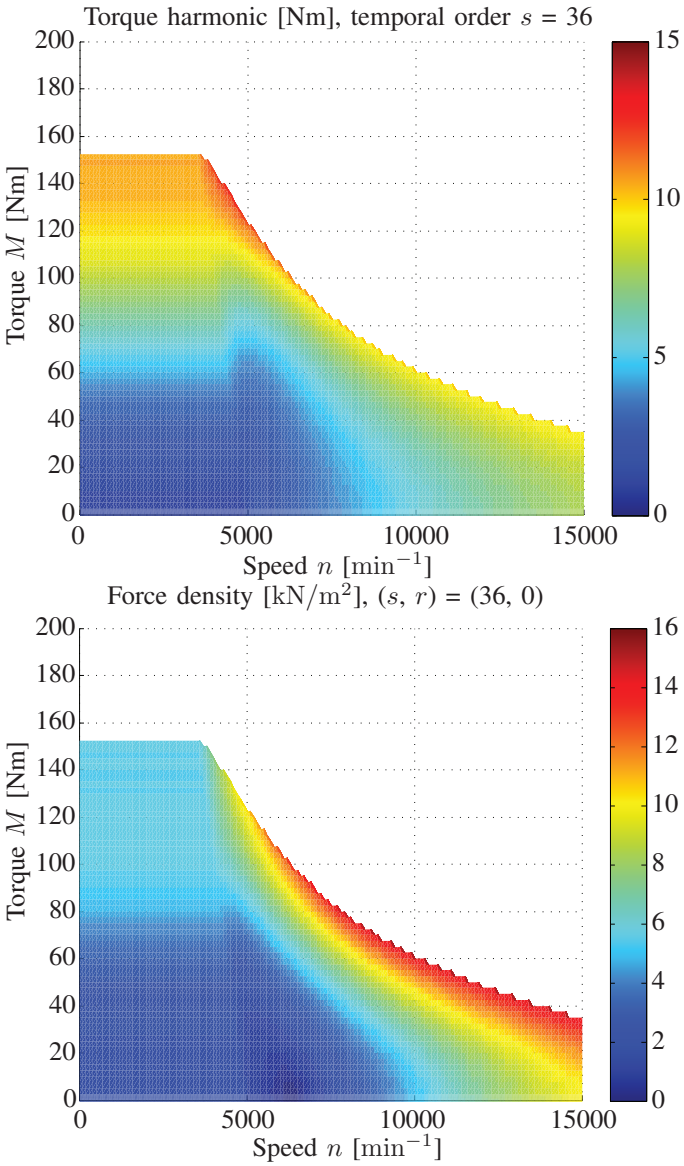

Fig. 11: Characteristic torque-speed-diagram of the 36$^{\mathrm{th}}$ torque harmonic (top) and the force density order (temporal s, spatial r) = (36, 0) (bottom).

B. Analysis of the Entire Operating Area

In Fig. 11 the characteristic torque-speed-diagram of the 36$^{\mathrm{th}}$ torque harmonic and the radial force density wave order (36, 0) are shown. Due to the change of reluctance, the maximum torque of the IPMSM is reduced by 2.5 Nm. The 36$^{\mathrm{th}}$ torque harmonic at its shifted rated speed $n = 3600\,\mathrm{min}^{-1}$ is 11.27 Nm, which represents 7.4 % of the mean torque. The maximum value of the radial force density order (36, 0) is 15 kN/m^2 at $n = 9600\,\mathrm{min}^{-1}$ and $M = 65\,\mathrm{Nm}$.

VI. Conclusions

It is shown, that through the alteration of the rotor surface, the harmonics of the air gap flux density can be reduced. This correlates with the distribution of the force densities acting on the stator teeth, which are responsible for the noise emission. The noise reduction is obtained by the reduction of the relevant force density order and thus the related surface velocities. The combination of sinusoidal field pole and notch in q-axis shows the most promising results. In this case, the relevant torque harmonic 36$^{\mathrm{th}}$ and radial flux density order (36, 0) are reduced at least by 58 %.

References

[1] S. A. Gelfand, *Essentials of Audiology*, Thieme Medical Publishers, 2009.

[2] D. Franck, M. van der Giet, K. Hameyer, "Towards low audible noise drives for FEV applications", in *14th International Power Electronics and Motion Control Conference (EPE/PEMC)*, 2010, S11-25 - S11-30.

[3] H. Jordan, *Geräuscharme Elektromotoren*, W. Girardet, 1950.

[4] R. Richter, *Elektrische Maschinen: Allgemeine Berechnungselemente*, Birkhäuser, 1951.

[5] R. De Doncker, D. Pulle, A. Veltmann, *Advanced Electrical Drives: Analysis, Modeling, Control*, Springer, 2010.

[6] G. Müller, K. Vogt, B. Ponick, *Berechnung elektrischer Maschine*, Wiley-VCH Verlag GmbH, Weinheim, 2008.

[7] J. Gieras, C. Wang, J. C. Lai, *Noise of Polyphase Electric Motor*, CRC Press Taylor & Francis Group, 2006.

[8] M. van der Giet, R. Rothe, M.H. Gracia, K. Hameyer, "Analysis of noise exciting magnetic force waves by means of numerical simulation and a space vector definition", *18th International Conference on Electrical Machines (ICEM)*, 2008.

[9] F. Henrotte, M. Felden, M. van der Giet, K. Hameyer, "Electromagnetic force computation with the Eggshell method", *Proc. 14th International Symposium on Numerical Field Calculation in Electrical Engineering (IGTE)*, 2010.

[10] S. Huang, J. Liu, J. Gao, L. Xiao, "Optimal design of the rotor structure for interior permanent magnet synchronous motor", in *Proc. International Conference on Power Engineering, Energy and Electrical Drives (PowerEng)*, 2011, pp. 1-5.

[11] K.-W. Jeon, T.-Y. Lee, Y.-J. Kim, S.-Y. Jung, "Numerical shape design characteristics of torque ripple reduction for Interior Permanent Magnet Synchronous Motor", in *Proc. 9th IET International Conference on Computation in Electromagnetics (CEM)*, 2014, pp. 1-2.